Book of Tutorials and Abstracts

European Microbeam Analysis Society

EMAS 2025

18th

EUROPEAN WORKSHOP

on

MODERN DEVELOPMENTS AND APPLICATIONS IN MICROBEAM ANALYSIS

11 to 15 May 2025
at the
TecnoCampus
Mataró (Barcelona), Spain

Organized in collaboration with the
Universitat de Barcelona, Spain

EMAS
European Microbeam Analysis Society eV
www.microbeamanalysis.eu/

This volume is published by:
European Microbeam Analysis Society eV (EMAS)
EMAS Secretariat
c/o Eidgenössische Technische Hochschule, Institut für Geochemie und Petrologie
Clausiusstrasse 25
8092 Zürich
Switzerland

ISBN 978 90 8227 6985
NUR code: 972 – Materials Science

TOWARDS ABSOLUTE LOCAL STRESS MEASUREMENTS THROUGH NON-SIMULATION-BASED HIGH ANGULAR RESOLUTION EBSD

Tijmen Vermeij[1,2], L.R. Dodsworth[1], A. Winkelmann[3], R. de Kloe[4] and J.P.M. Hoefnagels[1]

1 Eindhoven University of Technology, Dept. of Mechanical Engineering
Gemini Building 15, Groene Loper, 5612 AE Eindhoven, The Netherlands
2 Empa - Swiss Federal Laboratories for Materials Science and Engineering, Laboratory for Mechanics of Materials and Nanostructures
Feuerwerkerstrasse 39, 3602 Thun, Switzerland
3 AGH University of Krakow, Academic Centre for Materials and Nanotechnology (ACMiN)
Al. A. Mickiewicza 30, PL-30059 Krakow, Poland
4 Ametek BV, EDAX/Gatan Business Unit
Ringbaan Noord 103, P.O. Box 4144, NL-5004 JC Tilburg,The Netherlands
e-mail: tijmen.vermeij@empa.ch

Tijmen Vermeij obtained his PhD (Cum Laude) in Mechanical Engineering from Eindhoven University of Technology (TU/e), focussing on the micromechanics of plasticity and damage in advanced steels. He is currently a postdoctoral researcher at Empa in Thun (Switzerland), where his research involves developing and applying nano- and micromechanical in situ testing techniques, including electron backscatter diffraction (EBSD), transmission Kikuchi diffraction (TKD), combined with digital image correlation (DIC). In parallel, since his master's thesis, for which he received the TU/e Best MSc Thesis Award, he has been working on advancing high-resolution electron backscatter diffraction (HR-EBSD) methods. He has authored 19 publications in peer-reviewed scientific journals.

1. ABSTRACT

Over the years, high angular resolution electron backscatter diffraction (HR-EBSD) has evolved into a reliable tool for measuring misorientations and relative elastic strains in crystalline materials with high sensitivity. However, in the absence of strain-free intragranular reference points, absolute elastic strain measurements are not yet routinely performed and methodology developments are ongoing in the literature. Virtually all efforts involve the use of strain-free simulated EBSD patterns as a reference. However, in this work, we explore the potential of extracting the absolute elastic strain state from an experimental EBSD pattern without using any reference, except for (parts of) the pattern itself. An advanced integrated digital image correlation framework is proposed and employed to correlate multiple regions within the pattern with each other, exploiting crystal symmetry and plane-stress conditions. Using only a single pattern, we identify the absolute elastic strain state, the crystal orientation and the pattern centre and we demonstrate sensitivity levels close to that of traditional relative HR-EBSD. This is demonstrated on virtual patterns and on stress-free experimental patterns, for which we apply dedicated excess-deficiency correction routines.

2. INTRODUCTION

Sub-grain 'micro- to nano-scale' spatial resolution elastic stress/strain measurement techniques using high-angular resolution electron backscatter diffraction (HR-EBSD) have been explored for over 15 years, starting from the relative HR-EBSD method by Wilkinson *et al.* [1]. Such frameworks allow for the computation of all relative deviatoric elastic strain components [1, 2], with a relative elastic strain resolution below 10^{-4} on experimentally obtained electron backscatter diffraction patterns (EBSPs) [3].

In order to obtain absolute elastic strain measurements in the absence of a strain-free reference point in the same grain, kinematically and eventually more computationally expensive dynamically simulated EBSPs [4] were used as strain-free reference patterns. Tanaka *et al.* [5] were able to drastically cut the computation time of such a so-called simulation-based HR-EBSD technique by rapid computation of individual dynamically simulated EBSPs through interpolation of a pre-simulated master EBSD pattern [6]. However, simulation-based HR-EBSD still faces severe limitations. In all current simulation-based HR-EBSD frameworks, the pattern centre (PC) and strain state cannot be fully determined simultaneously [7], without making further assumptions on the strain state or employing more advanced correlation routines. As a result, for simulation-based HR-EBSD techniques, both PC and detector distance (DD) have to be determined beforehand using other methods, such as a Hough-transform or moving screen technique. Deviations in this determination will lead to strain errors, referred to as "phantom strains", which for these conventional calibration techniques are approximately 10^{-3} [4], effectively negating the strain accuracy. Tanaka *et al.* [5] were able to decrease these "phantom strains" to below $6*10^{-4}$, using a PC calibration step using a strain-free reference pattern

obtained in the same sample, resulting in a strain accuracy below 10^{-3} on experimental patterns. However, this does not only require that there is a strain-free point in the sample, but because the PC calibration relies on a supposedly strain-free experimental reference pattern, the technique by Tanaka *et al.* [5] cannot be considered fully absolute.

Recently, Vermeij *et al.* [8] proposed a framework for absolute stress measurements in HR-EBSD without using simulated patterns as reference, i.e., absolute non-simulation-based HR-EBSD. This framework demonstrated, for the first time, an absolute strain accuracy below 10^{-4} in a virtual case study on dynamically simulated EBSPs. By co-correlating the pattern centres of multiple EBSPs originating from different grains, fully exploiting crystal symmetry and plane-stress inside an advanced integrated digital image correlation (IDIC) framework [9], the PC, DD, crystal orientation and the stress state could be simultaneously determined. Consequently, this framework does not experience ”phantom strains” and its strain accuracy is thus not limited by ”phantom strains”.

This promising non-simulation-based framework does however have its challenges. The strain accuracy ($< 10^{-4}$) was only obtained in a virtual case-study on dynamically simulated EBSPs, and some factors observed in experimental EBSPs may cause additional stress errors. These factors include: energy variations over the EBSD pattern, stress variation within the EBSD interaction volume, optical distortions, deviations in relative PC location, noise and the excess-deficiency (E/D) effect. Accordingly, validation of the stress/strain accuracy on experimental EBSPs is required, which is the main goal of this work. However, before conducting this validation, the framework and the experimental setup were modified to decrease the effects of the experimental error sources. This was done through the following modifications with associated (potential) benefits:

- Single-pattern correlation: This removes the effects of uncertainties in relative PC locations on the stress/strain accuracy. Single pattern correlations also allow experimental validation on reliable single-crystal silicon samples.
- Direct-electron-detector EBSPs: EBSPs obtained using a direct electron detector are sharper and include no optical distortions.
- Validation on strain-free samples: In this work experimental validation will be done on near stress/strain-free single-crystal silicon samples which can be assumed to be strain-free because the residual stresses are much smaller than the usual assumed stress sensitivity. Because only strain-free samples will be used, the stress variations inside the EBSD interaction volume are also eliminated.

Through the above-mentioned modifications, all possible experimental error sources, except for the E/D effect, are likely either minimised or removed. It is thus hypothesised that the E/D effect will be the main source of stress/strain errors in the modified non-simulation-based framework for experimental direct-electron-detector EBSPs. The E/D effect is caused by the forward bias of inelastic backscattering events, which causes an anisotropic distribution of the inelastically scattered electrons with respect to the incident beam direction [10]. This creates an asymmetry

in intensity across the two edges of the same Kikuchi band. A brighter edge, i.e., the excess line, and a darker edge, i.e., deficiency line, are situated on respectively the top and bottom of a Kikuchi band. Because of the direction of sample tilt, the E/D effect is most pronounced in the Kikuchi bands perpendicular to the incident beam direction, i.e., horizontal bands, and (nearly) absent in Kikuchi bands parallel to the incident beam direction, i.e., vertical bands.

The first part of this paper will show that E/D effects are indeed the main source of stress/strain errors in experimental EBSPs, which is shown with the help of a dynamically simulated pattern with a simulated E/D effect, where this simulated E/D effect is determined through a fit on the corresponding experimental pattern.

The second part of this paper will discuss a strategy to reduce this error, caused by the E/D effect. This is done through an integrated E/D correction in the modified non-simulation-based framework, which aims at reducing the E/D effect in the pattern through a subtraction of an optimised correction field approximating the experimental E/D effect. It will be shown that in combination with further adjustments on the experimental setup, aimed at reducing the E/D effect, a strain accuracy below 10^{-3} can be achieved for experimental strain-free single-crystal silicon samples.

3. SINGLE-PATTERN CORRELATION FRAMEWORK

3.1. Methodology

Here, an absolute HR-EBSD technique is proposed that aims to determine PC, DD, crystal orientation and the absolute stress tensor, without the need for a simulated pattern as a reference while only using a single pattern, i.e., single-pattern absolute non-simulation-based HR-EBSD.

The proposed framework is based on the non-simulation-based framework by Vermeij *et al.* [8], which fully exploits the IDIC-based framework proposed in [9], as well as a plane stress assumption and full crystal symmetry to achieve a final absolute strain accuracy below 10^{-4} on non-E/D simulated patterns in a virtual case study. By assuming the plane stress and using crystal symmetry, the sensitivity of the framework is enhanced, which makes absolute stress measurements possible. These different parts were integrated in the IDIC framework by Vermeij *et al.* [35] as follows. Through crystal symmetry, multiple sets of two overlapping, theoretically identical, global regions of interest (gROIs) can be identified. All these overlapping gROIs, in multiple EBSPs originating from different grains, are correlated together to allow for the simultaneous determination of PC, DD, crystal orientation and even the absolute stress state if a plane stress condition is assumed. The here-proposed framework is very similar, but instead of using multiple patterns from different grains, only one patterns is used, leading to the structure described and explained below. This explanation will be aided by Fig. 1, which schematically shows how crystal symmetry creates sets of theoretically identical gROIs inside the same EBSP.

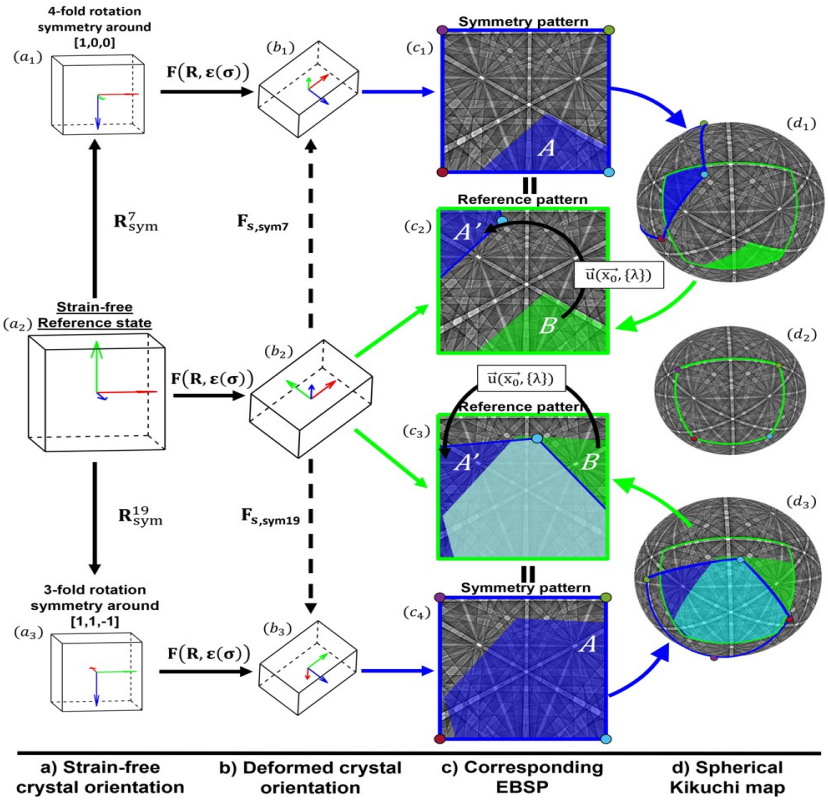

Figure 1. Example gROIs resulting from exploiting crystal symmetry. The red, green and blue axis in the crystal unit cells represent the x, y and z axis respectively. The areas highlighted and outlined in green and blue correspond with respectively the reference and the two symmetry patterns, which are all the same deformed pattern at the detector (with each corner point with a unique colour), while the cyan highlighted area denotes the overlap of areas highlighted in green and blue. For visualisation purposes the stretch of the deformed crystal orientation (column b) is exaggerated.

Consider a field of grey values representing the reference pattern, which is shown in Figs. 1c2 and 1c3, with the reference pattern outlined in green. This reference pattern originated from a crystalline material point with a certain deformed crystal orientation, shown in Fig. 1b2. This deformed crystal orientation can be described by a rotation tensor and a stretch tensor, that itself depends on a strain tensor, applied to a strain-free reference state of the crystal, such a strain-free reference state is shown in Fig. 1a2. The total deformation from the reference to the deformed crystal can be summarised by an absolute deformation gradient tensor.

Depending on the crystalline material, this strain-free reference state can be subjected to a certain number of symmetry operators. In this work, a silicon crystal is used which, due to its cubic unit cell, can be subjected to 24 symmetry operators. Each of these symmetry operators includes both a rotation and a reflection symmetry operator. In Figs. 1a1 and 1a3, the crystal orientations after application of 4-fold rotation symmetry around [1 0 0] and 3-fold rotation symmetry around [1 1 -1] are shown respectively.

When these strain-free crystal orientations, which were subjected to crystal symmetry operators, are subjected to the same deformation as the reference state, the same view of the crystal from the detector screen is found, as shown in Figs. 1b1 and 1b3. Because the view of the crystal on the detector screen is the same for deformed crystals with and without an applied symmetry operator, the corresponding patterns, respectively the reference and symmetry patterns, are identical, as shown in column c in Fig. 1. However, as shown by the coloured axis in column b, the rotation and deformation of the deformed crystals corresponding with the reference (Fig. 1b2) and symmetry (Figs. 1b1 and 1b3) patterns are different. This difference in rotation and deformation means that when these patterns are projected back onto a spherical Kikuchi map, as shown in column d of Fig. 1, they do not occupy the same area. In column d of Fig. 1, the projected reference and symmetry pattern are highlighted in respectively green and blue. This shows that any EBSP (as seen at the detector) is present many times on the Kikuchi sphere (48 times for silicon) due to rotational and reflection symmetry (which is well known in the literature).

Depending on the PC, DD, crystal irientation and stress state of the reference pattern, for certain symmetry operators the reference and symmetry pattern overlap on the Kikuchi sphere. This is the case for both symmetry operators selected for Fig. 1, where the overlapping area in d1 and d3 is highlighted in blue. This overlapping area is seen in both the reference and symmetry patterns (column c). Because these regions occupy the same region on the Kikuchi sphere, they must be equal. Moreover, as shown in column c of Fig. 1, because of crystal symmetry, the view of the deformed crystal at the detector is the same for both the reference and symmetry configuration. Consequently, the reference and symmetry patterns are identical, meaning that area A in the symmetry pattern has to be equal to the same area B in the reference pattern, i.e., A = B. By combining the previous two statements, it is found that if the different rotation and deformation tensor are known, area A is equal to area B, creating a set of theoretically identical gROIs inside the reference pattern for each symmetry operator where an overlap between symmetry and reference pattern is observed.

However, the different deformation gradient tensors, dependent on the stress state and crystal rotation, and parameters such as PC and DD, are not well known. These uncertainties create brightness residuals between the two corresponding areas (A and B) for each symmetry operator. The HR-EBSD/IDIC framework makes it possible for multiple gROIs corresponding to the different symmetry operators to be correlated together in a consistent full-field one-step optimisation approach as to determine PC, DD, crystal orientation and the absolute deviatoric stress state through the simultaneous minimisation of all these brightness residuals.

All experimental patterns are acquired from silicon single crystals at 20 kV employing an EDAX Clarity direct electron EBSD detector. All simulated patterns, with and without E/D effects, are simulated with dynamical many-beam simulations, see more details in Winkelmann *et al.* [10-12]. Simulations were performed to match the experimental patterns as closely as possible.

The assumptions and the math as presented in [8] and [9] is employed for all correlations. Notably, ε_{11} needs to be constrained to 0, similarly to the framework in [8]. Discussions on this and improvements for this will be briefly discussed at the end of this paper.

3.2. Results

Fig. 2 shows the strain errors for non-E/D simulated, E/D simulated and experimental patterns. Herein, the good convergence for non-E/D simulated pattern can be observed, with a maximum strain error below $3*10^{-5}$, which is comparable to the stress/strain accuracies found by the multi-pattern non-simulation-based framework on non-E/D simulated patterns in a virtual case study [8]. However, as shown in Fig. 2 for experimental patterns, the strain accuracy is much worse, with a maximum strain error below $5*10^{-3}$, which suggests that an effect observed in experiments but not included in the non-E/D simulated patterns caused this large strain error. As shown in Fig. 2, for a E/D simulated pattern, which is a non-E/D simulated pattern with an added simulated E/D effect, a maximum strain error just below $4*10^{-3}$ is observed. This strain error closely resembles the strain error found for experimental patterns, with the strain error of an E/D simulated pattern being between 80 % and 100 % of the strain error found for the experimental pattern with the same geometry configuration. This suggests that the E/D effect is the main cause of stress/strain errors for this single-pattern non-simulation-based HR-EBSD framework. As such, the first step towards increasing the accuracy is by correcting for the E/D effect.

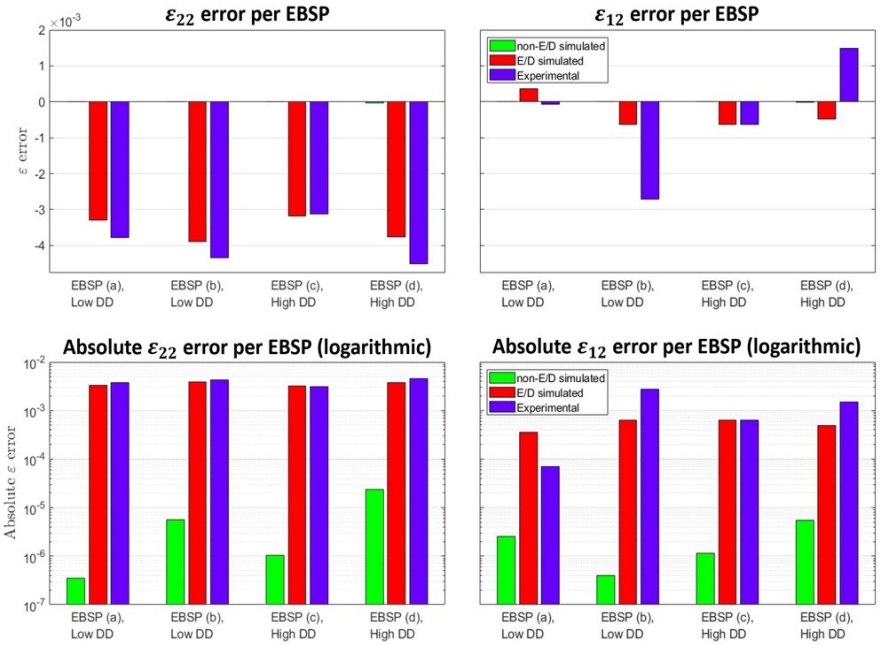

Figure 2. Errors on a linear (top) and logarithmic scale (bottom) for the three types of analysed patterns: Non-E/D simulated (green), E/D simulated (red) and experimental (blue). For the bar plots with logarithmic scale the absolute strain errors are shown.

4. *INTEGRATED E/D CORRECTION*

4.1. Extended correlation framework

As discussed by Winkelmann *et al.* [10], an experimental pattern can be approximated as the sum of an EBSP without E/D effect and a field describing the E/D effect. We approximate the experimental E/D effect using the gradient in y of the EBSP, as shown in Fig. 3a. This is based on earlier work by Winkelmann *et al.* [13], in which the gradient was used with added Gaussian blurring as a rough E/D correction in the preprocessing step. Besides blurring, we also need to account for spatial variations in the strength of E/D effects. This will be tackled by employing b-spline fields that are multiplied by the blurred y-gradient. These integrated corrections are combined into one E/D correction as shown in Fig. 3a (blue) in the form of a graphical flowchart, with the exact step where the combination of the corrections highlighted in red. Consequently, a number of DOFs are added, representing the b-spline field and the degree of blurring. These DOFs will be co-correlated with the rest of the parameters (related to the absolute orientation, strain and PC).

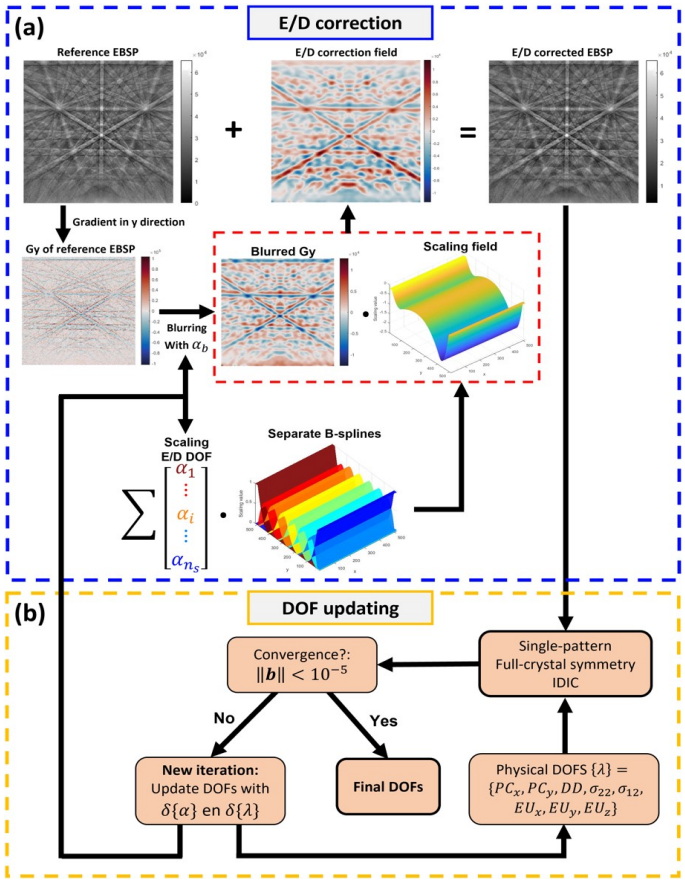

Figure 3. Flowchart describing the working principle of the E/D correction in the single-pattern non-simulation-based framework. a) Illustration of how E/D correction is applied on the EBSP using the updated E/D DOFs. b) Illustration on how the added E/D DOFs.

The E/D corrected non-simulation-based framework optimises the original DOFs through minimisation of the brightness residual, which assumes conservation of brightness over the entire EBSD. This is accomplished by the integrated correction of the experimental E/D effect through the added optimisation of the E/D DOFs. The E/D correction is achieved in the form of a brightness relaxation, the concept of which is described in detail in [9, 14].

4.2. Initial E/D correction results

In Fig. 4 the strain errors of the E/D corrected and non-E/D corrected single-pattern non-simulation-based framework are compared for both E/D simulated and experimental patterns. For both the E/D simulated and experimental patterns the ε_{22} error decreases due to E/D correction. Overall, E/D correction on the experimental pattern outperforms E/D correction on E/D simulated patterns. However, the reduction in overall strain error after E/D correction for both E/D simulated and experimental patterns is fairly limited, especially when compared to the results of non-ED simulated patterns. This seems to suggest that there are inaccuracies in the E/D correction field.

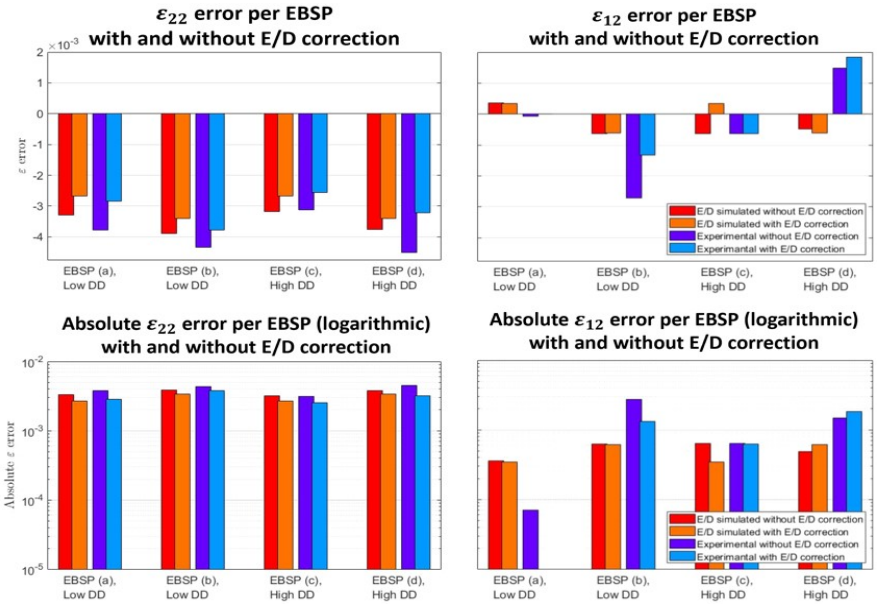

Figure 4. Comparison of strain errors on a linear (top) and logarithmic scale (bottom) for E/D simulated and experimental patterns, with and without E/D correction. All results are taken after convergence of both the E/D DOFs and physical original DOFs.

Extensive effort was applied into optimisation of the E/D correction framework, but no significant improvements were made. As such, we investigated several clear Kikuchi bands at varying locations in the pattern (not shown here) and we found that the E/D correction performed

better on the top part of the pattern, where the E/D effect was less strong. Accordingly, the next step is to assess the possibility of using a smaller part of the pattern (on the top) to perform the correlations.

4.3. Experimental adjustment for E/D corrections

Here, we explore the possibility of excluding certain regions from the IDIC correlation, for which numerical E/D correction is unable to properly approximate and subsequently correct the E/D effects.

The effect of the high E/D effect observed in the bottom of the EBSP, for which the E/D correction performs less accurately, can be removed by not including the bottom of the EBSP into the correlation. Ideally, this is achieved by moving the detector up, i.e., by capturing an EBSP with a lower PCy, whereby a smaller region with high E/D effect below the PC and a larger regions with less E/D above the PC is captured, keeping nearly the same amount of total data. While we would expect reduced signal for such geometries, most IDIC frameworks are very robust to noise [8, 9, 14]. The framework is thus well equipped to robustly correlate these lower E/D effect EBSPs with a lower PC and higher noise at the top part of the EBSP.

However, during this work, no SEMs were available that were capable of moving the detector screen up enough to not include any of these high E/D effect regions. Consequently, in this paper, to show the capabilities of our single-pattern correlation method, the lower part of the EBSP will be excluded from the correlation. This limits the amount of useful data, here quantified by the amount of available symmetry operators. Accordingly, we employ these correlations on patterns with a low DD, i.e., a high capturing angle, in order to assure that we have enough pattern to correlate.

4.4. Results and discussion

To assess the efficacy of using a smaller part of the pattern, we assess the performance of the correlation as a function of the amount of pattern used. We define this by the "cut-off angle", as illustrated in Fig. 5c. This angle denotes the amount of pattern used in y direction, starting from the PC. Figs. 5a and 5b show the absolute strain error, and its range (over multiple patterns), for respectively ε_{22} and ε_{12}, for different cut-off angles. Additionally, the total data that is included in the correlation for these different cut-off angles is visualized in Fig. 5d through the amount of used symmetry operators.

Fig. 5a shows that both the average and the maximum absolute ε_{22} error initially decreases when more of the lower part of the EBSP is excluded from the correlation, with a minimum at ~ 25° cut-off angle below the PC with a maximum ε^{22} error below $5*10^{-4}$. A further decrease in the cut-off angle results in a wider strain error range for the different sample rotations, which can

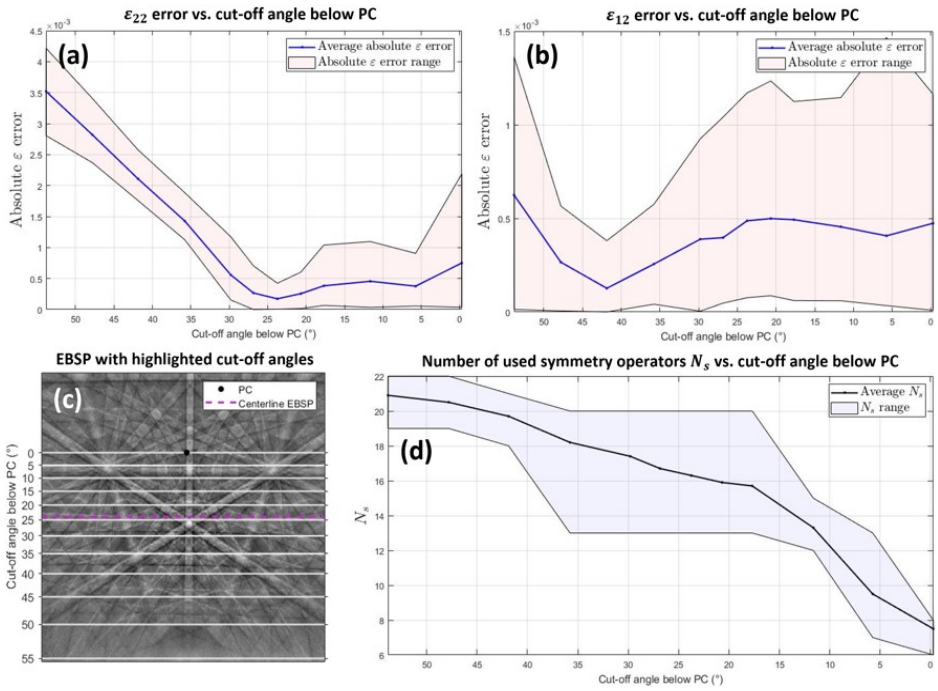

Figure 5. Average absolute error and absolute error range for a) ς22 and b) ς12, over all low DD EBSPs, from the E/D corrected single-pattern non-simulation-based framework for different cut-off angles below the PC. (c) Cut-off angles visualised on the experimental EBSP shown in Fig. 2.1.a, with a visualised PC and the vertical centreline of the EBSP which was used as the cut-off location in section 2.5. d) Range and average of the amount of used symmetry operators Ns over all low DD EBSPs for different cut-off angles below the PC.

be attributed to the decrease in the total amount of correlation data, as visualised in Fig. 5d. For the average and maximum ε_{12} error, shown in Fig. 5b, initially a similar trend is seen, up to a higher cut-off angle of ~ 40° with a maximum error also below $5*10^{-4}$, with increases in error again for higher angles.

Overall, for the patterns discussed in this paper, a cut-off angle of 27° results in the best overall maximum strain accuracy, which is just below $1.1*10^{-3}$.

5. *CONCLUSIONS AND FUTURE WORK*

This paper proposed an extension on the original non-simulation-based framework of Vermeij *et al.* towards absolute stress measurements on a single pattern. We were able to simultaneously determine the PC, DD, crystal orientation and absolute stress/strain state with an absolute strain accuracy below 10^{-4} in a virtual case study on dynamically simulated patterns.

For experimental patterns (and more realistic simulations), E/D effects reduced the accuracy of the framework and therefore required extensive corrections. We tackled this by introducing an integrated E/D correction framework, which involves estimation of the E/D effect using the y-gradient and implementing it as a brightness-relaxation field. While effective, achieving high accuracies required an additional experimental correction in which only part of the pattern was used for the correlations. This showed that absolute strain errors below $5*10^{-4}$ are feasible for experiments.

Future work focuses on the determination of the full in-plane elastic strain tensor, because currently one of the in-plane normal strain components still needs to be constrained. Promising initial results have been attained by capturing and correlating an extra pattern, obtained using a different detector distance or by rotating the sample. The results of this will be presented during the EMAS workshop.

6. REFERENCES

[1] Wilkinson A J, Meaden G and Dingley D J 2006 *Ultramicroscopy* **106** 307-313
[2] Britton T B and Wilkinson A J 2011 *Ultramicroscopy* **111** 1395-1404
[3] Villert S, Maurice C, Wyon C and Fortunier R 2009 *J. Microscopy* **233** 290-301
[4] Britton T B, Maurice C, Fortunier R, Driver J H, Day A P, Meaden G, Dingley D J, Mingard K and Wilkinson A J 2010 *Ultramicroscopy* **110** 1443-1453
[5] Tanaka T and Wilkinson A J 2018 *Microsc. Microanal.* **24** 962-963
[6] Callahan P G and De Graef M 2013 *Microsc. Microanal.* **19** 1255-1265
[7] Alkorta J 2013 *Ultramicroscopy* **131** 33-38
[8] Vermeij T, De Graef M and Hoefnagels J 2019 *Scripta Materialia* **162** 266-271
[9] Vermeij T and Hoefnagels J P M 2018 *Ultramicroscopy* **191** 44-50
[10] Winkelmann A, Nolze G, Cios G, Tokarski T, Bała P, Hourahine B and Trager-Cowan C 2021 *J. Microscopy* **284** 157-184
[11] Winkelmann A 2008 *Ultramicroscopy* **108** 1546-1550
[12] Winkelmann A, Trager-Cowan C, Sweeney F, Day A P and Parbrook P 2007 *Ultramicroscopy* **107** 414-421
[13] Winkelmann A, Jablon B M, Tong V S, Trager-Cowan C and Mingard K P 2020 *J. Microscopy* **277** 79-92
[14] Neggers J, Blaysat B, Hoefnagels J P M and Geers M G D 2016 *Int. J. Numer. Meth. Eng.* **105** 243-260